Testing and Analyses of Davis-Besse Alloy 600 Control Rod Drive Mechanism Nozzles

Technical Letter Report

Darrell S. Dunn

U.S. Nuclear Regulatory Commission
Office of Nuclear Regulatory Research

November, 2014

Contents

Tables

Figures

Executive Summary

In 2002, the original Davis-Besse reactor pressure vessel head (RPVH) was damaged by primary water stress corrosion cracking (PWSCC) of the alloy 600 control rod drive mechanism (CRDM) nozzle #3, followed by boric acid corrosion of the low alloy steel RPVH. At the time of the inspection, the RPVH had 15.8 effective full power years (EFPY) of operation. Subsequent testing of the alloy 600 material from CRDM nozzle #3 at Argonne National Laboratory (ANL) revealed measured crack growth rates that were above the 75 percentile of measured crack growth rates reported by industry showing that this material was susceptible to PWSCC. Although the measured crack growth rates were higher than the disposition curve for alloy 600, the microstructure of the alloy 600 material used in CRDM nozzles #1-5 was not consistent with material that would be expected to have above average PWSCC susceptibility.

After the 2002 inspection findings, the original RPVH was removed and replaced with the RPVH from the cancelled Midland, Michigan nuclear power plant. The replacement RPVH also had CRDM nozzles manufactured from alloy 600. In February 2010, PWSCC was identified during an inspection of alloy 600 CRDM nozzles in the replacement RPVH after only 5.5 EFPY. As a result, the licensee repaired 24 of the 69 CRDM nozzles prior to plant restart. In addition, in October 2011, the repaired RPVH was removed and replaced with an RPVH with alloy 690 CRDM nozzles.

Through-wall failures in both the original and the initial replacement RPVH occurred in a relatively short period of time compared to previous operating experience. In order to better understand the susceptibility of these materials, the NRC contracted ANL and Pacific Northwest National Laboratory (PNNL) to conduct confirmatory crack growth rate testing and the microstructural characterization related to the PWSCC of the alloy 600 CRDM nozzles. Crack growth rate testing showed that both alloy 600 heat M3935 used in the original RPVH and alloy 600 heat M7929 used in the replacement RPVH were more susceptible to PWSCC than other alloy 600 materials previously tested by NRC and industry. However, although both of the susceptible heats of alloy 600 were manufactured by the same vendor and were approximately of the same vintage, the alloy 600 nozzles used in the original and replacement RPVHs were found to have substantially different microstructures. In the original RPVH, fabricated from alloy 600 heat M3935, significant impurity segregation was observed along chromium depleted grain boundaries, which may have contributed to enhanced PWSCC susceptibility. The replacement RPVH, fabricated from alloy 600 heat M7929, was found to have microstructural factors that have been shown to increase PWSCC susceptibility, including a small grain size and few grain boundary carbides.

Acknowledgments

The author gratefully acknowledges the work of Jim Hyres at Babcock and Wilcox Technical Services in the preparation of specimens used in this study and the many helpful discussions with Jay Collins, Dave Alley, Rob Tregoning, and Mirela Gavrilas at the Nuclear Regulatory Commission.

Introduction

Primary coolant leakage as a result of PWSCC was observed in both the original and the initial replacement RPVH at the Davis-Besse nuclear power plant. The original RPVH (hereafter referred to as RPVH #1) had CRDM nozzles #1 - 5 manufactured from alloy 600 heat M3935. This heat of alloy 600 has been reported to be susceptible to PWSCC [1]. During an inspection in 2002, boric acid corrosion damage of the low alloy steel RPVH was discovered around CRDM nozzle #3 that had through wall leakage as a result of PWSCC [2]. At the time, RPVH #1 had 15.78 effective full power years (EFPY) of operation.

After PWSCC and boric acid corrosion was discovered in 2002, RPVH #1 was removed and replaced. The initial replacement RPVH (hereafter referred to as RPVH #2) was originally constructed for the cancelled Midland, Michigan plant and the control rod drive mechanism (CRDM) nozzles were also manufactured from alloy 600. Of the 69 CRDM nozzles in RPVH #2, 68 were manufactured from alloy 600 heat M7929.

During a scheduled refueling outage that began on February 28, 2010, an inspection of RPVH #2 revealed that twelve of the nozzles inspected did not meet acceptance criteria. Subsequent examinations showed PWSCC indications in 24 vessel head penetrations and associated welds, and boric acid deposits characteristic of active leakage on CRDM nozzle #4 [3]. Figure 1 shows a diagram summarizing the 2010 inspection results for RPVH #2. At the time of the February 2010 inspection, RPVH #2 had 5.5 EFPY of operation since the plant restart in March, 2004. Based on the results of base metal visual inspection (Figure 2), CRDM nozzle #4 was confirmed as a leaking nozzle. Ring samples were removed from CRDM nozzles #4 and #10 (alloy 600 heat M7929) and the affected nozzles were repaired prior to plant restart. In addition, the licensee provided the NRC with a 90 degree section of the ring sample removed from CRDM nozzle #4 for microstructural analyses and crack growth rate (CGR) testing.

This report summarizes the results of CGR testing and metallurgical analysis of alloy 600 heat M3935 from CRDM nozzle #1 of RPVH #1 and alloy 600 heat M7929 from CRDM nozzle #4 of RPVH #2. After decontamination, test specimens were machined from these CRDM nozzles by Babcock and Wilcox Technical Services (BWXT) under contract to the NRC. The prepared specimens were then provided to Pacific Northwest National Laboratory (PNNL) and Argonne National Laboratory (ANL) for CGR testing and metallurgical analyses. Measured CGRs and analyses were compared to the results for alloy 600 heat M3935 (nozzle #3 from RPVH #1) that was previously tested at ANL [4] and PNNL [5], and the disposition curve for alloy 600 proposed by the Electrical Power Research Institute (EPRI) [6]. Full details of all testing and analyses conducted by ANL and PNNL are included as attachments to this report.

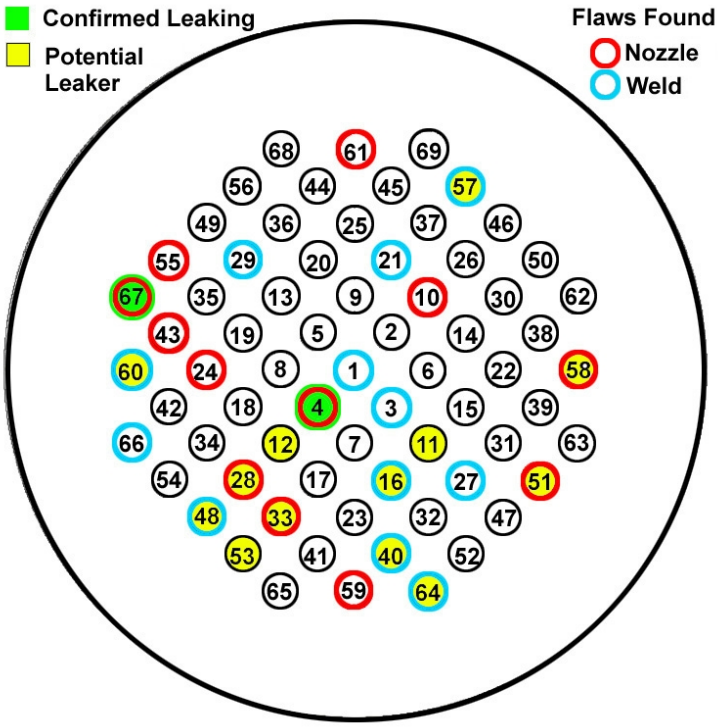

Figure 1. Results of the February 2010 inspection of the Davis-Besse RPVH after 5.5 EFPY of operation.

Figure 2. Bare metal visual inspection of Davis-Besse RPVH CRDM nozzle #4 showing the presence of boric acid deposits indicating possible leakage.

Test Materials

Alloy 600 heats M3935 from Davis-Besse RPVH #1 and M7929 from Davis-Besse RPVH #2 were examined in this study. The composition and mechanical properties of the alloys obtained from the certified material test reports (CMTRs) are provided in Tables 1 and 2. Both heats, manufactured by Babcock & Wilcox Tubular Products Division, meet the requirements for alloy 600 described in the American Society of Mechanical Engineers (ASME) Boiler and Pressure Vessel code specification SB-167 [7]. Detailed processing records for the two alloy 600 heats were not readily available but general information reveals that these heats were processed similarly. Xu et al. [1] reported that the processing of heat M3935 used an estimated final mill anneal temperature of 871 to 927°C (1600 to 1700°F) and that rough and final nozzle machining took place after the final mill anneal. Information available for heat M7929 is also limited and the only known requirement for this material was to maintain the final annealing temperature above 871°C (1600°F) for a minimum of 10 minutes. An annealing temperature as low as 885°C (1625°F) may have been used [3].

Table 1. Alloy 600 composition (weight percent unless noted)

Alloy 600 heat	Ni	Cr	Fe	Mn	C	P	Cu	Co	Si	S	B* appm
SB-167 Specification	72.0 min	14.0-17.0	6.0-10.0	1.0 max	0.15 max	N/A	0.5 max	N/A	0.5 max	0.015 max	N/A
M3935	77.89	15.58	6.25	0.27	0.028	0.004	0.01	0.01	0.37	0.0022	69
M7929	75.28	16.12	7.24	0.26	0.03	N/A	0.01	0.05	0.45	0.003	77

*Boron concentration measured by PNNL

Table 2. Alloy 600 mechanical properties and hardness

Alloy 600 heat	Yield Strength, MPa	Tensile Strength, MPa	Elongation, percent	Hardness, Vickers*		
				Min	Max	Ave ± SDEV
SB-167 Specification	205 min	550 min	35 min	N/A	N/A	N/A
M3935	334	590	60	146.6	190.7	160.2 ± 6.5
M7929	296	668	53	166.6	209.5	186.5 ± 9.6

*Hardness in the crack growth plane for M3935-RPVH #1-CRDM #1 and M7929-RPVH #2-CRDM #4 measured by PNNL

Initial fluorescent dye penetrant testing (PT) and dimensional measurements were obtained to determine the useable dimensions of the 90 degree section of heat M7929. The dimensions of the nozzle section and photographs taken during PT are shown in Figures 3 to 6. The PT test did not reveal any surface breaking flaws and allowed the entire nozzle section to be used to produce test specimens. A specimen layout was developed to determine possible compact tension (CT) specimen placement and orientation. Based on the nozzle section dimensions, both ¼T-CT and ½T-CT specimens could be machined (Figure 7). The ¼T- CT and ½T-CT specimens machined from the 90 degree section of heat M7929 are shown in Figure 8. The

available section of heat M3935 from CRDM nozzle #1 of RPVH #1 was much larger and multiple specimens were produced for testing and analyses.

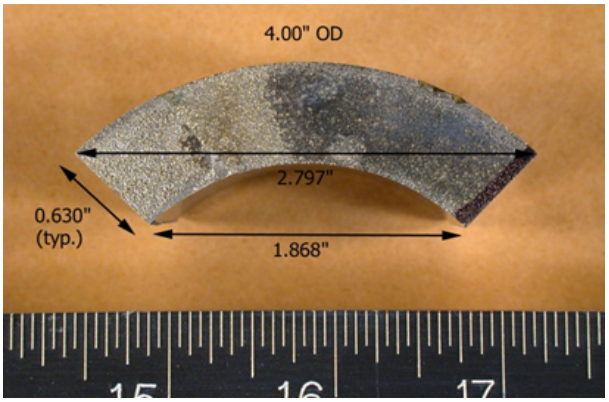

Figure 3. Top view of nozzle#4 section and dimensional measurements

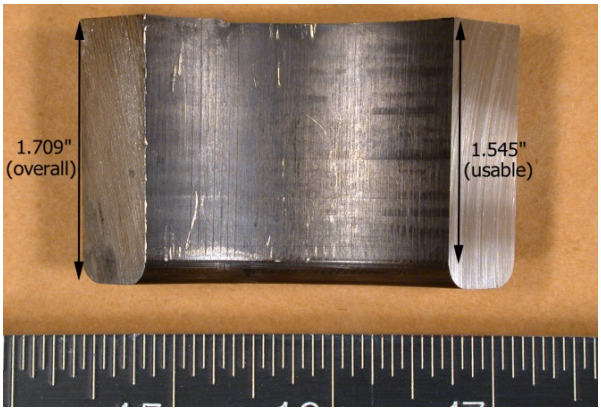

Figure 4. Inside diameter view of nozzle #4 section with dimensional measurements

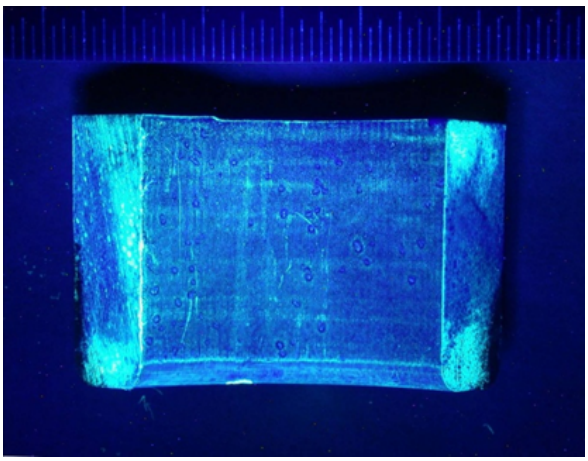

Figure 5. Black light photograph of the inside diameter surface during PT

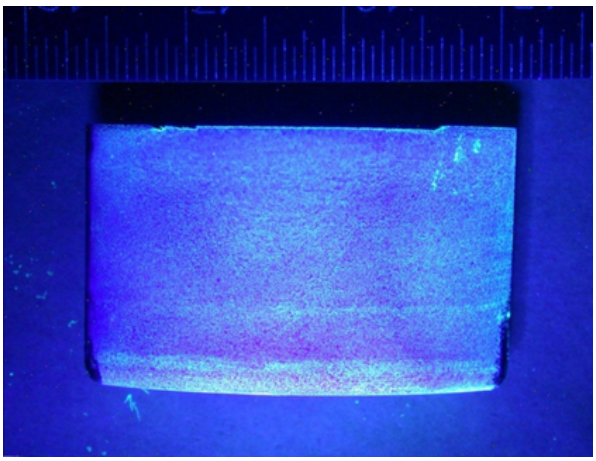

Figure 6. Black light photograph of outside diameter surface during PT

Sections of alloy 600 heats M3935 and M7929 were decontaminated prior to the completion of test specimen machining. Initial radiological survey results for heat M7929 indicated dose rates of 500 mR/hr on contact and 10 mR/hr at 30.5 cm (12 inches). Most radioactivity was likely due to surface contamination in the oxide layer of the inner surface of the nozzle sections. Removing the surface layers in the course of machining the specimens removed most of the contamination. After machining, final decontamination of the specimens was conducted using a potassium permanganate solution. The decontamination process was sufficient to allow all samples to be free releasable.

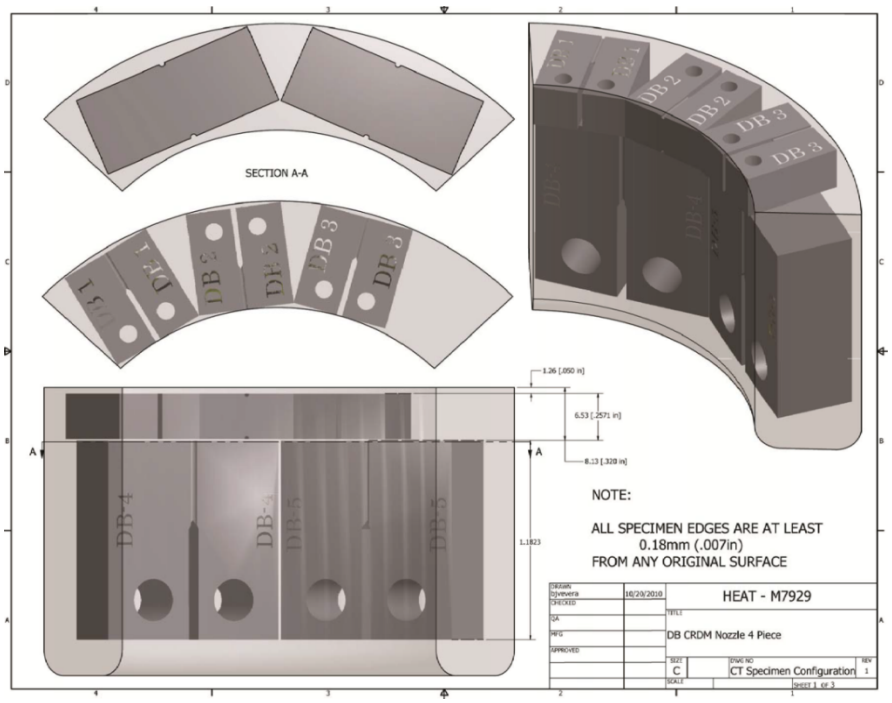

Figure 7. Computer-aided design (CAD) drawing showing final specimen layout for the CT specimens machined from alloy 600 heat M7925 (CRDM nozzle #4 of RPVH #2)

Figure 8. Alloy 600 heat M7925 compact tension test specimens and extra piece for metallurgical analyses (to the right of specimen DB-3) after machining and decontamination

This page intentionally left blank

Crack Growth Rate Testing

Crack growth rate testing was conducted at both ANL and PNNL in simulated PWR environments at temperatures of 290-360°C (554-680°F). For the most part, tests were conducted in accordance with American Society for Testing and Materials (ASTM) standards E-647 and E-1681 [8,9]. Details of the test systems and test management protocols have been previously described [4,10]. The simulated PWR primary water contained 1000 ppm boron and 2 ppm lithium. In addition, the temperature, pH, conductivity and hydrogen concentration of the water were carefully controlled and monitored. Specimens were mounted in autoclaves with appropriate fixtures for loading. The autoclaves were attached to load frames and the specimens were loaded using either servo-hydraulic or servo-electric actuators that were digitally controlled. Applied loads were measured with calibrated load cells and the specimen crack lengths were measured using direct current potential drop (DCPD) monitoring systems. A diagram of a CT specimen connected to a reversing DCPD system along with an actual image of a CT specimen loaded in the autoclave load fixture is shown in Figure 9. An image of an entire test system at ANL with the major components is shown in Figure 10.

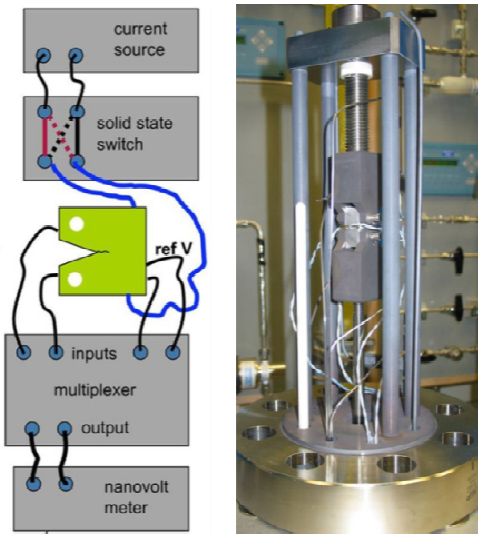

Figure 9. Schematic of reversing direct current potential drop systems to monitor crack length (left) and photo of compact tension specimens loaded into autoclave test fixture (right)

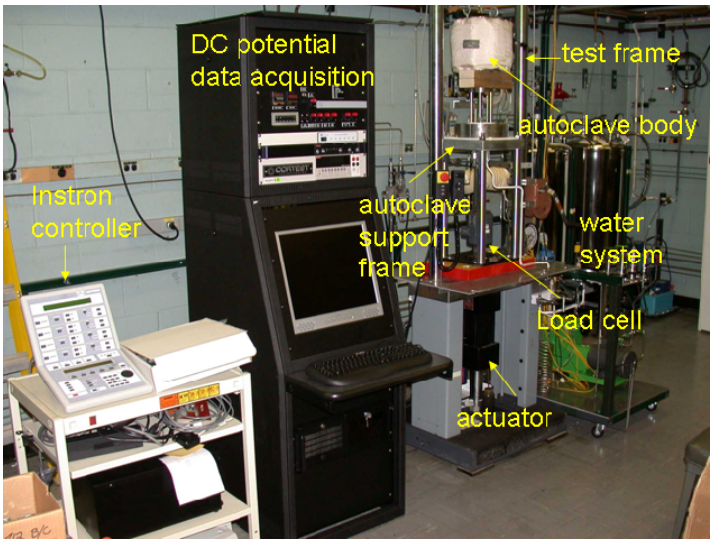

Figure 10. Laboratory system at ANL for conducting crack growth rate testing

A summary of the CGR measurements for the alloy 600 heats M3935 and M7929 are shown in Figure 11. Although CGRs under cyclic and cycle + hold conditions were obtained, only the constant stress intensity (K) or constant load CGRs are shown in Figure 11. The ANL data for heat M3935 from CRDM #3 was previously reported in NUREG/CR-6921 [4]. This material had

measured CGRs that were above the 90th percentile for alloy 600 based on disposition curves developed by the Electrical Power Research Institute (EPRI) Materials Reliability Program (MRP) [6]. Testing of alloy 600 heat M3935 at PNNL was conducted using compact tension specimens machined from CRDM nozzle #1 of RPVH #1. As shown in Figure 9, the crack growth rates reported by PNNL for alloy 600 heat M3935 were between the 25th and 75th percentile crack growth rate disposition curves reported in EPRI MRP-55 [6].

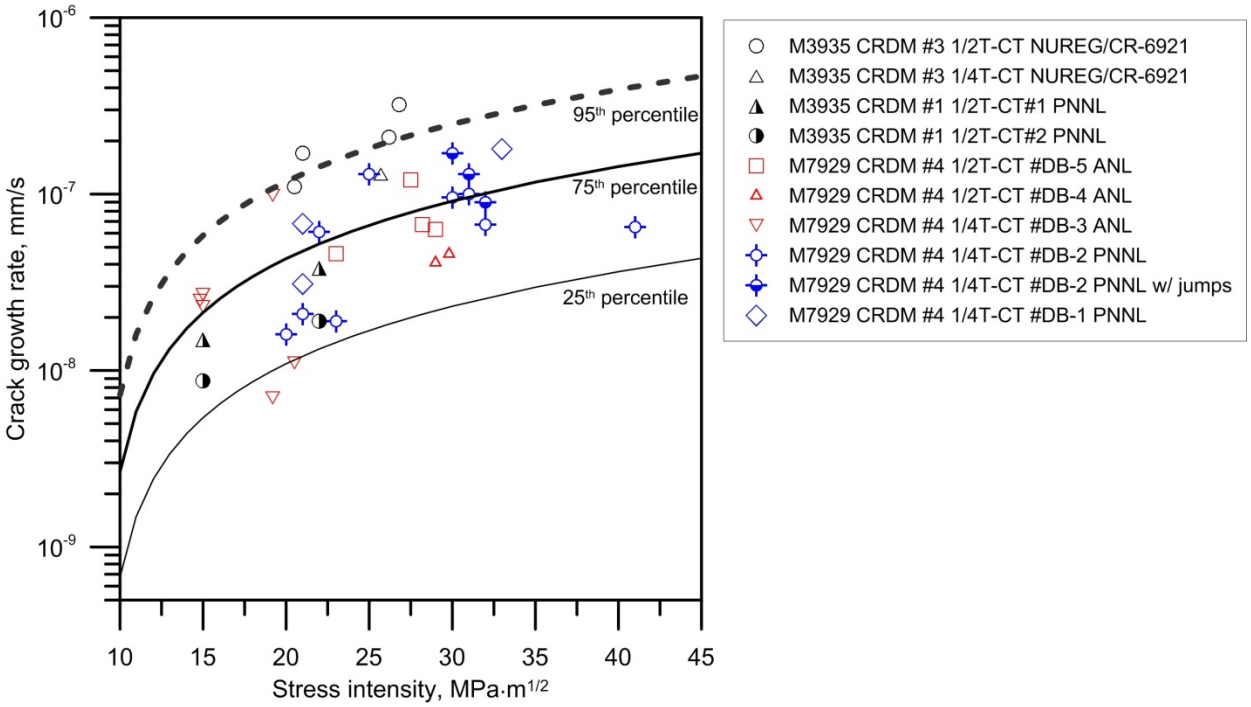

Figure 11. Crack growth rate test results for Davis-Besse alloy 600 heats M3935 and M7929

Specimens DB-3, DB-4 and DB-5 (see Figures 7 and 8) of alloy 600 heat M7929 from RPVH #2 were tested at ANL. These specimens displayed a tendency to form ligaments or small sections of material behind the main crack front that were not fractured. The formation of ligaments behind the advancing crack front occurs under constant load conditions and cyclic loading tends to break the ligaments and straighten the crack front. Cyclic loading after prolonged time at constant load resulted in a higher than the expected cyclic CGR and was interpreted as the breaking of ligaments that formed under constant load conditions. The formation of ligaments affects DCPD measurement of crack length and artificially lowers the measured CGRs. To account for this effect, the crack length measured by DCPD was adjusted to include the rapid crack length increase observed under cyclic loading after long constant load CGR measurements. Taking the formation of ligaments into account, the M7929 specimens tested at ANL had crack growth rates that varied between the 25th to the 95th percentile of the alloy 600 crack growth rates.

An example of the methodology for determining the actual crack growth rate and compensating for the formation of ligaments is shown in Figure 12. During this test, periods 14 and 16 are under identical loading conditions (cycle plus 2 hour hold) and therefore the crack growth rate should also be identical. However after a long period of constant load crack growth rate measurement in period 15, the crack propagation rate under cycle plus hold loading in period 16 was substantially higher than expected for approximately 400 hours. Afterwards, the crack growth rate slowed to the expected value of 6 × 10^{-10} m/s. The dotted line in Figure 10, drawn to connect the initial crack length at the start of period 15 to the crack length in period 16 where the rate under cycle plus hold loading reached the expected value. The adjusted crack growth rate for period 15 is determined by dividing the crack advance compensated for the formation of ligaments divided by the time under constant load conditions. In this case, the DCPD crack growth rate was measured to be 3.2×10^{-11} m/s and the adjusted rate was 1.3×10^{-10} m/s.

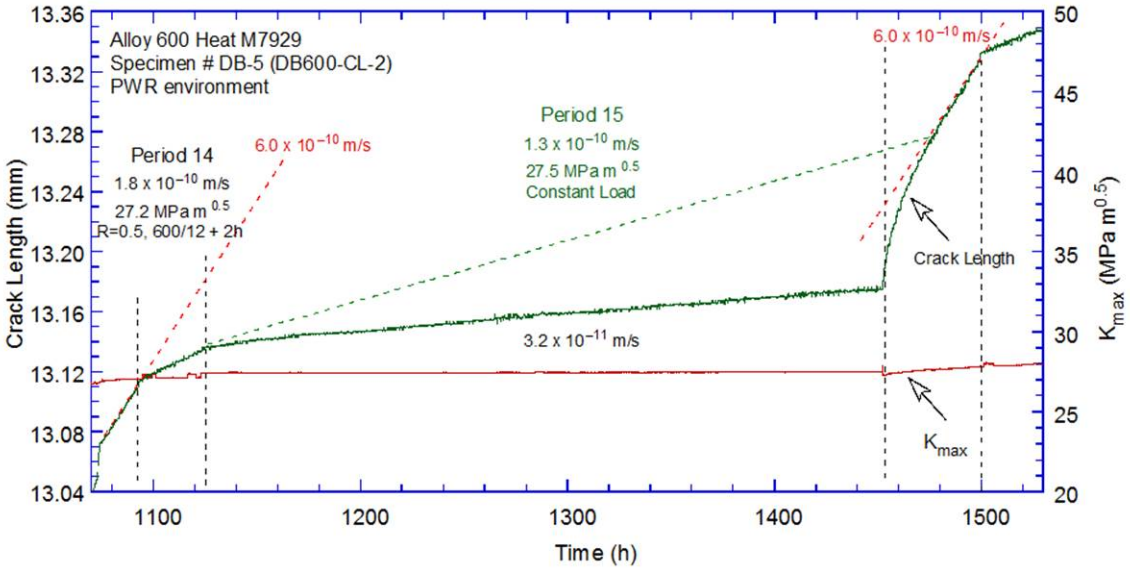

Figure 12. Crack growth rate testing of Alloy 600 heat M7929 at ANL showing the measured DCPD crack growth rate and the adjusted rate to compensate for the effects of ligaments formed under constant load conditions

Results of the measured CGRs for Alloy 600 heat M7929 specimens tested at PNNL also showed some scatter with rates between the 25th and 95th percentile CGRs for alloy 600 reported in MRP-55 [6]. Tests conducted with ¼T-CT specimen DB-2 showed periodic jumps in crack length under constant K conditions and following constant K conditions when cyclic loading was applied. Consistent with the interpretation of the testing conducted at ANL, these observations were attributed to the formation and breaking of ligaments. Crack growth rates for specimen DB-2 with and without these sudden jumps are shown in Figure 11. Without taking the jumps into consideration, the measured CGRs were in some cases at the 75th percentile disposition curve [6] but with the jumps considered the measured CGRs were considerably higher.

An example of the measured crack growth rates obtained at PNNL are shown in Figure 13. As indicated periodic jumps in the crack length were observed under constant K conditions. Cyclic loading at the end of a long period of constant K CGR testing sometimes resulted in significant crack advance in a few cycles. The formation of a ligament under constant K conditions that is broken in subsequent cyclic loading is the most plausible explanation for these observations.

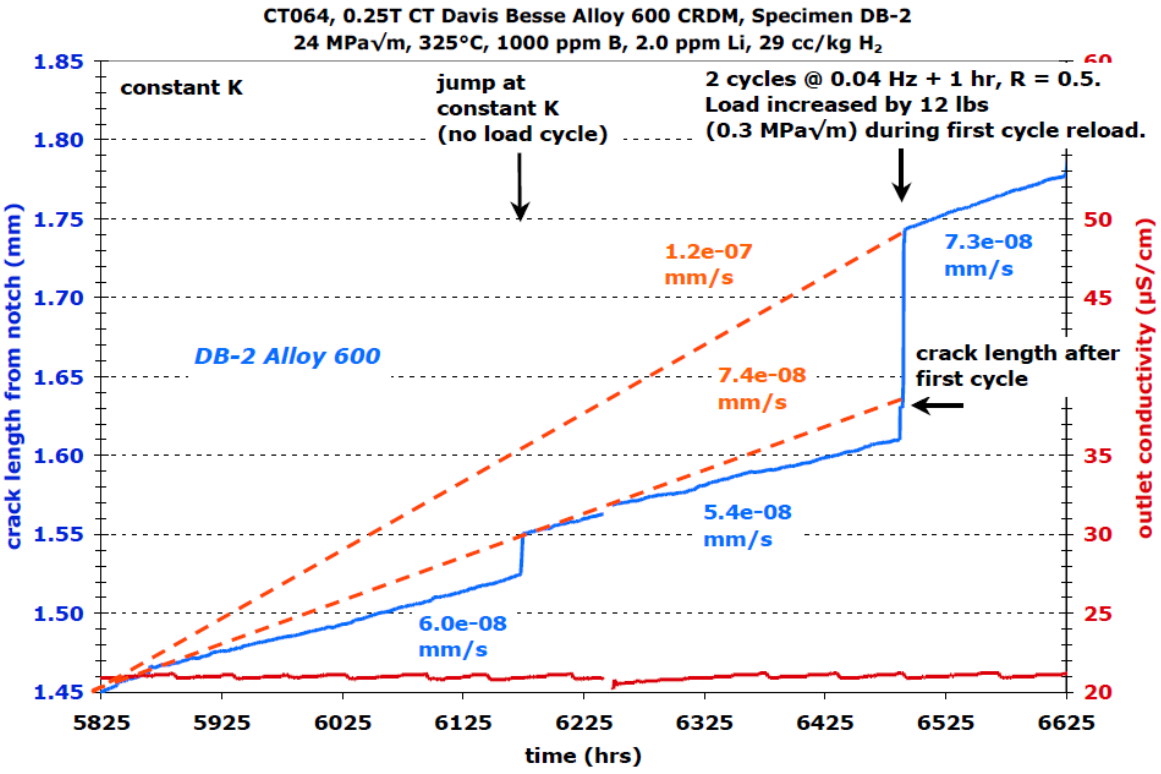

Figure 13. Crack growth rate testing of Alloy 600 heat M7929 at PNNL showing the measured DCPD crack growth rate and the sudden increase in crack length attributed to the breaking of ligaments

The fracture surfaces of heat M3935 were predominately intergranular and ANL reported that the transition from a transgranular fatigue crack to an intergranular crack occurred very readily [4]. Similarly, the fracture surface from heat M7929, specimens DB-5 and DB-4 tested at ANL also showed a high degree of intergranular engagement when the crack path and fracture surfaces were examined after testing. Similar fracture surfaces were obtained with the heat M7929 CT specimens tested at PNNL. Details of these examinations and images of the fracture surfaces are described in the attached reports from ANL and PNNL. The significant intergranular engagement of the M7929 heat provides additional evidence that this heat is susceptible to PWSCC. Nevertheless, the measured CGRs for both the M7929 heat were not noticeably greater than the originally measured CGRs for the M3935 heat obtained from CRDM #3 of RPVH #1 that was previously reported by ANL [4].

Metallurgical Analyses

A summary of the metallurgical analyses of the M3935 and M7929 heats are shown in Table 3. The M3935 heat (Figure 14) had 200 to 400 μm diameter grains. The grain boundaries were decorated with carbides and the carbide spacing was from 500 to 700 nm. In contrast, the M7929 heat (Figure 15) exhibited a 15 to 30 μm grain size and carbides were predominately transgranular located on what appeared to be prior grain boundaries. This is evident in Figure 13 where the red arrows show grain boundaries and the blue arrows show the carbides.

The previous analysis conducted by ANL [4] indicated that the alloy 600 heat M3935 in CRDM nozzle #3 from RPVH #1 had a grain size varied from 30 to 200 μm, with an average size of approximately 75 μm (ASTM grain size 4). Extensive grain boundary coverage (GBC) by Cr–rich carbides was reported along with some carbides randomly distributed in the matrix. In most cases, the carbides appeared to be present only on one side of the grain boundary. The average size of the grain boundary carbides was ≈0.3 μm, and the GBC was estimated to be in the range 50–60%.

Elemental composition of the grain boundary regions in both alloy 600 heats using atomic probe tomography (APT) is shown in Figure 16. Significant chromium depletion was observed at the grain boundaries in heat M3935 reaching a value of about 6 atomic percent. Minor chromium depletion was observed at certain grain boundary locations near well-spaced chromium carbides in heat M7929 reaching levels down to 12 atomic percent. Slight intergranular enrichment of phosphorus, manganese and titanium was also identified. In both heats, significant enrichment of boron was discovered with measured grain boundary concentrations of ~6 and ~2.7 atomic percent for M3935 and M7929, respectively. It is important to note that APT underestimates boron measurements due to trajectory errors and the actual grain boundary concentration is greater than these values. A more complete description of the APT results is reported elsewhere [11].

Table 3. Alloy 600 microstructural analyses summary

Component	Alloy 600 Heat #	Grain Size (μm)	Primary Carbides	Carbide Density	Grain Boundary Cr Composition (atomic %)	Grain Boundary B Composition (atomic %)
RPVH #1 CRDM Nozzle #1	M3935	200 - 400	Intergranular	500-700 nm spacing	6	6
RPVH #2 CRDM Nozzle #4	M7929	15 - 30	transgranular (on ghost grain boundaries)	High	12	2.7

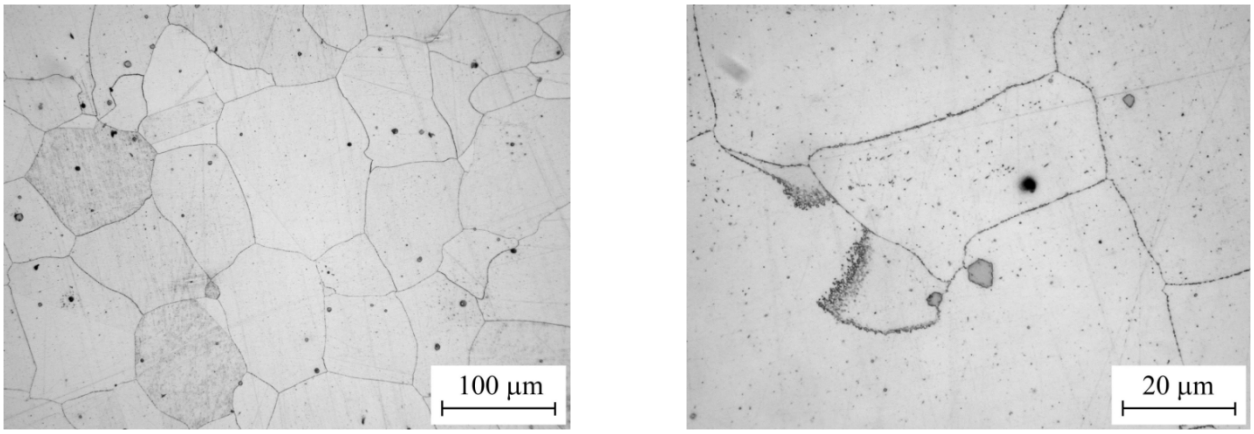

Figure 14. Microstructure of the Davis-Besse RPVH #1 CRDM nozzle #3 (Alloy 600 heat M3935) at two magnifications [4]

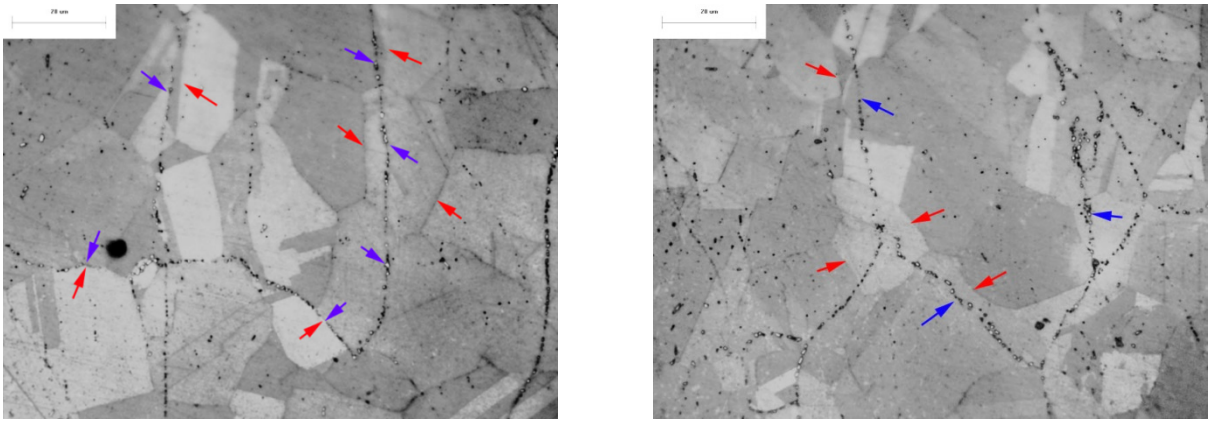

Figure 15. Microstructure of the Davis-Besse RPVH #2 CRDM nozzle #4 (alloy 600 heat M7929). Red arrows indicate grain boundaries and blue arrows indicate carbides. Scale bar 20 µm [0.0008 in]

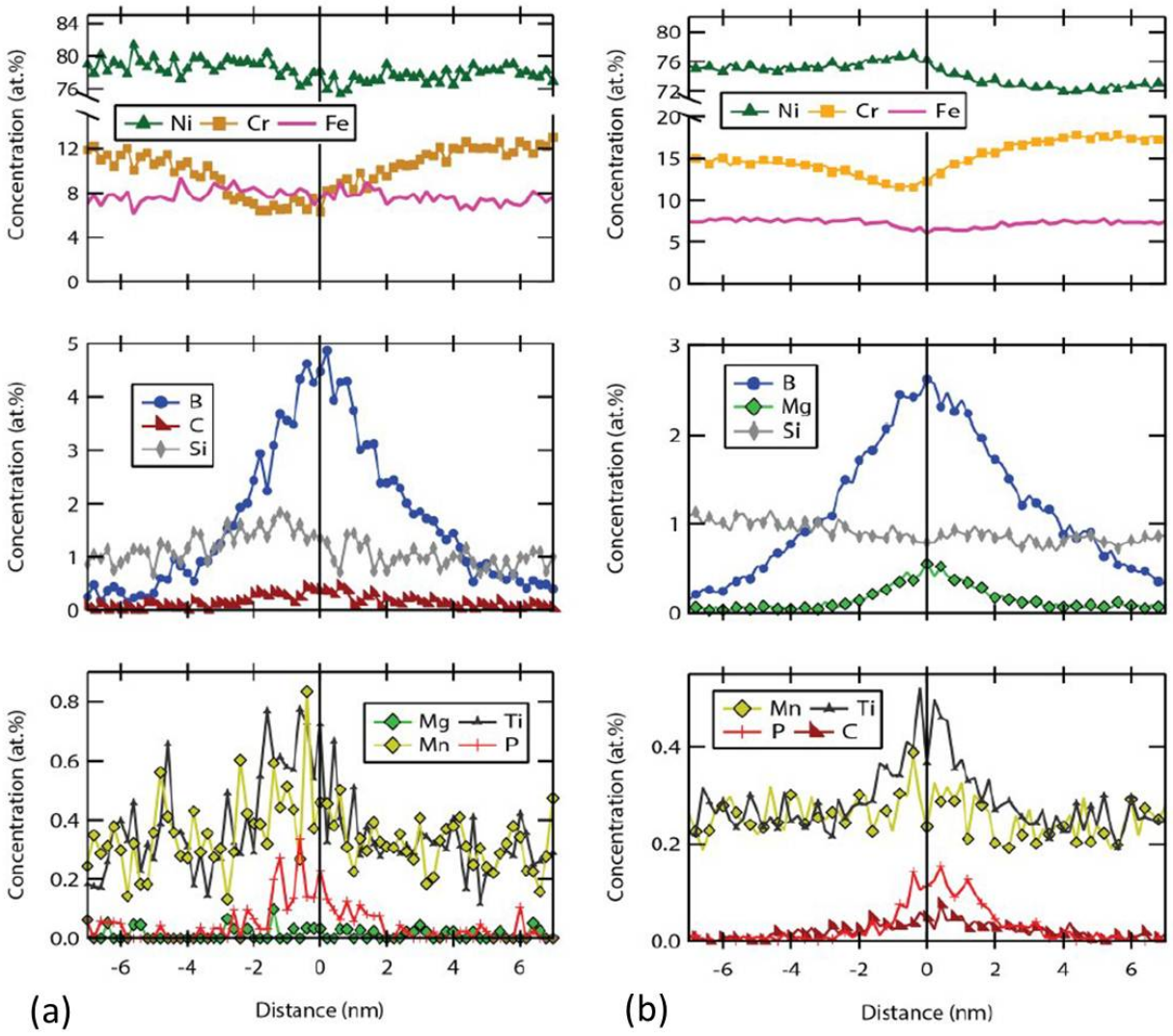

Figure 16: Concentration profiles across metal/metal grain boundary of alloy 600 (a) heat M3935 and (b) heat M7929. Boron, titanium, manganese and phosphorous segregation were observed in both heats. Significant chromium depletion was noted at most grain boundaries in heat M3935 associated with intergranular chromium carbides. Only limited chromium depletion was observed for heat M7929.

This page intentionally left blank

Discussion

The measured CGRs confirmed that both heats M3935 and M729 of alloy 600 from RPVH #1 and RPVH #2, respectively, were susceptible to PWSCC. Even though both heats exhibited similar CGRs in lab tests, their microstructures were quite different. Alloy 600 heat M7929 was found to have small grain size and to be devoid of grain boundary carbides. Carbide precipitates were located on ghost grain boundaries suggesting that the mill anneal temperature or time at temperature was insufficient to put carbides into solution. Both the M7929 and the M3935 heats both had significant grain boundary enrichment of boron along with minor enrichment of phosphorous and a few other elements. A high density of chromium carbides and grain boundary chromium depletion was also observed in heat M3935. It is of interest to understand the factors that affect PWSCC susceptibility of these two heats, particularly the possible influence of microstructure and grain boundary composition. Previous studies on the effects of grain boundary chemistry on PWSCC susceptibility are limited and the effects of boron or phosphorus enrichment are unclear as is the influence of grain boundary chromium depletion. Nevertheless the results of several investigations have been reported that offer insight into the individual and combined effects of microstructure, segregation and grain boundary composition on SCC.

Previous work has shown that both grain size and grain boundary carbide coverage affect both initiation of PWSCC and caustic cracking susceptibility of alloy 600 [12-17]. Norring et al. [12] tested a number of alloy 600 heats with a range of processing conditions and conducted PWSCC testing in hydrogenated water at 365°C (689°F) using reverse u-bends from steam generator tubing. The time to SCC initiation for mill annealed tubing was strongly dependent on annealing temperature in the range from 925 to 1025°C (1697 to 1877°F). Initiation times increased by a factor of 10× for materials annealed at 1025°C (1877°F) compared to material annealed at 925°C (1697°F). Lower annealing temperatures resulted in higher yield strength and smaller grain size along with decreased PWSCC initiation times. Longer time to initiation was also observed in mill annealed alloy 600 with increased grain boundary carbide coverage. Sung and Was [13, 14] showed that the fraction of intergranular cracking in 30 percent cold worked materials was greater in materials with a smaller grain size. Gomez-Briceno et al. [15] conducted initiation tests using ovalized tube samples in primary water at 330°C (626°F) and steam at 400°C (752°F) and reported that the time to failure decreased with both decreasing grain size and reduced grain boundary carbide coverage. Economy et al. [16] conducted testing using reverse U-bend specimens in hydrogenated steam at 400°C (752°F). Time to failure and the fraction of failed specimens with test time was strongly dependent on thermal treatment conditions. Mill annealed materials failed in as little as 200 hours whereas no failures of thermally treated materials occurred until 2400 hours of exposure. Bruemmer and Henager [17] also noted that mill annealed alloy 600 was more susceptible to intergranular SCC compared to both the thermally treated materials that have a semi-continuous distribution of grain boundary carbides and the solution annealed material with no grain boundary carbides. They proposed that a combination of microstructural and microchemical effects promote intergranular SCC. Materials in the solution annealed and mill annealed condition have few grain boundary carbides that can be activated as dislocation sources to relieve stresses along the grain

boundary ahead of an advancing crack. However, Bamford and Foster [18] reported that yield strength, grain size and carbide precipitate coverage had no effect on the crack growth rates of 15 heats of alloy 600 head penetration archive materials. Based on the testing and analyses of heat M7929 and the results of previous investigations, it appears very likely that the principal factor that led to failure of the CRDM nozzles in RPVH #2 was the alloy processing that resulted in a susceptible microstructure and rapid initiation of PWSCC. The observation that the crack growth rates for the M3935 and M7929 heats were similar is not inconsistent with the results of this previous testing of alloy 600 [18].

The measured grain boundary phosphorous enrichment was shown by Bruemmer and Was [19] to increase with decreasing heat treatment temperature and reached values near 30 atomic percent in alloy 600 after a heat treatment at 600°C (1112°F). Was et al. [20] reported that phosphorous segregates to the grain boundaries after thermal treatment at 700°C (1292°F). Because thermally treated alloy 600 is generally more resistant to PWSCC compared to the mill annealed material, it appears unlikely that phosphorous enrichment is strongly detrimental to PWSCC resistance. Sung and Was [13,14] performed constant extension rate tensile testing in high purity water at 360°C (680°F) with controlled purity alloy 600 heats with additions of phosphorous, carbon and boron. Addition of phosphorous and a thermal treatment that resulted in 5 percent phosphorous enrichment at grain boundaries decreased the fraction of intergranular cracking compared to a control material with no added impurities. The combination of carbon and phosphorous additions also decreased intergranular cracking. The amount of phosphorous enrichment measured in the M3935 and M7929 heats is considered to be minor and insufficient to cover a substantial fraction of the grain boundaries. Based on the analytical results and previous investigations, phosphorous enrichment at grain boundaries likely had no significant role in the PWSCC susceptibility of the two alloy 600 heats examined in this study.

Boron, which is sometimes added to increase hot workability [21], also segregates to grain boundaries. The effect of boron enrichment on SCC and intergranular corrosion of alloy 600 has been the subject of some debate. Boron has been reported to increase grain boundary cohesion [22] which suggests that boron enrichment would not promote intergranular SCC by embrittlement of the grain boundaries. Jones and Bruemmer [23] reported that the effect of boron on intergranular corrosion and SCC appears to be related to the chromium carbide precipitation kinetics. Low bulk levels of boron retard precipitation while higher levels accelerate precipitation. Thus, boron may affect SCC susceptibility in environments in which intergranular carbide precipitation and chromium depletion are instrumental in the cracking processes. Newman et al. [21] showed that boron increased the depth of intergranular corrosion of alloy 600 in caustic solutions at 350°C (662°F). Sung and Was [13,14] showed that additions of carbon and boron in a high purity alloy 600 solution annealed heat treatment at 600°C (1112°F) for 250 hours resulted in grain boundaries with a high degree of boron enrichment (8.8 percent) and chromium depletion to 6 atomic percent but no intergranular cracking during constant extension rate tensile testing in high purity water at 360°C (680°F). However, Schreiber et al. [11] analyzed grain boundary composition in several alloy 600 heats and suggested that boron or silicon enrichment may promote SCC. Schreiber et al. [11] also reported that boron was selectively dissolved from the grain boundaries after exposure to PWR primary water at

temperatures of 325 – 330°C (617 – 626°F). Stiller et al. [24] tested several alloy 600 heats and the most susceptible materials had considerable grain boundary boron enrichment. In comparison to the susceptible materials tested by Stiller et al. [24], the M3935 heat has approximately twice the grain boundary boron concentration. While the results of previous studies do not provide a clear picture on the effects of grain boundary boron enrichment, it appears possible that intergranular attack as a result of the elevated boron concentration in heat M3935 may be a factor in the PWSCC on RPVH #1.

By itself, chromium depletion of the heat M3935 grain boundaries was not likely a factor in the PWSCC in RPVH #1 based on numerous previous studies including the results reported by Sung and Was [13,14] and Stiller et al. [24]. Scarberry et al. [25] concluded that deaerated water or alkaline environments do not attack Cr depleted areas and grain boundary precipitates may block cracking; however, in environments that are capable of promoting intergranular attack as a result of chromium-depleted regions, the application of a stress may promote SCC. This was demonstrated with sensitized alloy 600 in polythionic acid solutions at room temperature. It should be noted that Thomas et al. [5] reported sulfur-rich spots in reacted carbide interfaces during previous analyses of stress-corrosion cracks in heat M3935 from Davis-Besse RPVH #1 CRDM nozzle #3; however, no sulfur enrichment was found in the examination of the microstructure of heat M3935 from RPVH #1 nozzle #1. Based on the presence of sulfur at stress-corrosion crack tips, Thomas et al. [5] suggested that sulfur impurities in the primary water environment may have helped promote PWSCC in the Davis-Besse RPVH #1.

This page intentionally left blank

Conclusions

Two alloy 600 heats that were in service at the Davis-Besse nuclear power plant were shown to be susceptible to PWSCC. Both heats were supplied in the mill annealed condition but had significantly different microstructures. Heat M3935 had 200 to 400 micron grains and grain boundaries with carbide precipitates. Analyzed grain boundaries had significant enrichment of boron and minor enrichment of phosphorus along with chromium depletion. While there are conflicting reports in the literature, it appears that the PWSCC susceptibility of the M3935 heat may be related to the effect of significant boron enrichment at grain boundaries with extensive Cr depletion. While contamination of the primary water may have occurred in service, results of crack growth rate tests indicate this alloy 600 heat was susceptible to SCC in PWR primary water without the presence of sulfur species.

Heat M7929 had considerable enrichment of boron and minor enrichment of phosphorus at grain boundaries, but no significant chromium depletion. The notable microstructural characteristics of heat M7929 were small grain size and a significant fraction of grain boundaries that were devoid of carbide precipitates. The microstructure of heat M7929 is characteristic of alloy 600 heats that have been shown to decrease PWSCC initiation times and likely led to rapid initiation and through wall cracking of the M7926 CRDM nozzles in Davis-Besse RPVH #2.

This page intentionally left blank

References

1. H. Xu, S. Fyfitch and J.W. Hyres, Proceedings of the 12th International Conference on Environmental Degradation of Materials in Nuclear Power Systems—Water Reactors, G.T.R. Allen, P.J. King and L. Nelson, eds., TMS, pp. 833-842, 2005.

2. NRC Information Notice 2002–11, Nuclear Regulatory Commission, March 12, 2002.

3. A.T. Boland, Letter to A. Barry, October 22, 2010, NRC ADAMS ML102930380, 2010.

4. B. Alexandreanu, O.K. Chopra and W.J. Shack, NUREG/CR-6921, Nuclear Regulatory Commission, 2005.

5. L. Thomas, B.R. Johnson, J.S. Vetrano and S.M. Bruemmer, Proceedings of the 12th International Conference on Environmental Degradation of Materials in Nuclear Power Systems—Water Reactors, G.T.R. Allen, P.J. King and L. Nelson, eds., TMS, pp. 567-577, 2005.

6. PWR Materials Reliability Program Alloy 600 Issues Task Group, MRP-55, Revision 1, Electric Power Research Institute, Palo Alto, CA, 2002.

7. American Society for Mechanical Engineers Boiler and Pressure Vessel Code, Section II, Part B, SB-167, New York, NY, ASME, 2010.

8. American Society for Testing and Materials, E647-08, West Conshohocken, PA, ASTM, 2008.

9. American Society for Testing and Materials, E1681-03,West Conshohocken, PA, ASTM, 2008.

10. S.M. Bruemmer, and M.B. Toloczko, NUREG/CR-7103 Vol. 1. Nuclear Regulatory Commission, 2011.

11. D.K. Schreiber, M.J. Olszta, L.E. Thomas and S.M. Bruemmer, “Grain Boundary Characterization of Alloy 600 Prior To and After Corrosion by Atom Probe Tomography and Transmission Electron Microscopy,” Proceedings of the 16th International Conference on Environmental Degradation of Materials in Nuclear Power Systems—Water Reactors, G.O. Ilevbare, P. Andresen, and M. Wright, eds., NACE International, 2013.

12. K. Norring, J. Engstrom and P. Norberg, Proceedings of the 3rd International Symposium on Environmental Degradation of Materials in Nuclear Power Systems—Water Reactors, G.J. Theus and J.R Weeks, eds., The Minerals, Metals and Materials Society, pp. 587-593, 1987.

13. J.K. Sung and G.S. Was, Proceedings of the 4th International Symposium Environmental Degradation of Materials in Nuclear Power Systems—Water Reactors, D. Cubicciotti, ed., NACE, Houston, pp. 6-25 to 6-37, 1991.

14. J.K. Sung and G.S. Was, Corrosion Vol. 47(11), pp. 824-834. 1991.

15. D. Gomez-Briceno, F. Blazquez and F. Hernandez, Corrosion, Vol. 55(3), pp. 248-258, 1999.

16. G. Economy, R.J. Jacko and F.W. Pement, Corrosion, Vol. 43(12), pp. 727-734, 1987.

17. S.M. Bruemmer and C.H. Henager, Jr., Scripta Metallurgica, Vol. 20, pp. 909-914, 1986.

18. W.H. Bamford and J.P Foster, EPRI TR-109136, Palo Alto, CA, Electrical Power Research Institute, December 1997.

19. S.M. Bruemmer and G.S Was, Journal of Nuclear Materials, Vol. 216, pp. 348-363, 1994.

20. G.S. Was, H.H. Tischner and R.M. Latanision, Metallurgical Transactions A Vol. 12A, pp. 1397-1408, 1981.

21. J.F. Newman, P. McIntyre and S.M. Payne, EPRI NP-5971, 1987 EPRI Workshop on Secondary Side Intergraular Corrosion Mechanisms: Proceedings, pp. A11-1 – A11-37, 1987.

22. G.A. Young Jr., R. Najafabadi, W. Strohmayer, D.G. Baldrey, B. Hamm, J. Harris, J. Sticht and E. Wimmer, LM-03K047, Lockheed Martin, June 16, 2003.

23. R.H. Jones and S.M. Bruemmer, Environment-Induced Cracking of Metals, NACE-10, R.P. Gangloff and M.B. Ives, eds., pp. 287-310, 1990.

24. K. Stiller, J.O. Nilsson and K. Norring, Metallurgical and Materials Transactions A-Physical Metallurgy and Materials Science, Vol. 27(2), pp. 327-341, 1996.

25. R.C. Scarberry, S.C. Pearman and J.R. Crum, Corrosion, Vol. 32(10), pp. 401-406, 1976.